NASA TN D-1400

TECHNICAL NOTE

D-1400

INDUCED INTERFERENCE EFFECTS ON A FOUR-JET VTOL CONFIGURATION WITH VARIOUS WING PLANFORMS IN THE TRANSITION SPEED RANGE

By James H. Otis, Jr.

Langley Research Center
Langley Station, Hampton, Va.

NATIONAL AERONAUTICS AND SPACE ADMINISTRATION

WASHINGTON September 1962

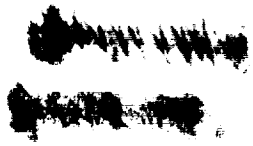

1A

NATIONAL AERONAUTICS AND SPACE ADMINISTRATION

TECHNICAL NOTE D-1400

INDUCED INTERFERENCE EFFECTS ON A FOUR-JET VTOL CONFIGURATION WITH VARIOUS WING PLANFORMS IN THE TRANSITION SPEED RANGE

By James H. Otis, Jr.

L
2
0
7
2

SUMMARY

An investigation of mutual interference out of the region of ground effect between a nozzle system, various wing-body combinations, and the free stream has been conducted in the Langley 300-MPH 7- by 10-foot tunnel. A series of wings with various planforms were tested in combination with a basic fuselage employing four convergent nozzles directed vertically downward (normal to the free stream). The nozzle configuration simulated the exhaust from a high-bypass-ratio turbofan propulsion system.

The jet-induced download and associated pitching moment were measured independently of the primary thrust by means of three strain-gage beams which attached the wing-body combination to the nozzle assembly. The data were obtained with the model at zero angle of attack at two different jet-exit velocities through a range of velocity ratios (free-stream velocity to average jet-exit velocity). A jet-induced download was encountered by all configurations throughout the velocity-ratio range with an accompanying nose-up pitching moment at velocity ratios greater than 0.1.

INTRODUCTION

Much interest has been generated recently in pure-jet VTOL aircraft built around high-bypass-ratio turbofan engines (refs. 1 and 2). This type of system generally employs four movable nozzles that rotate from the take-off position (jet exhaust directed vertically downward) rearward to the cruise condition. By this means the fuselage remains horizontal during take-off and landing. The transition from hovering to forward flight is accomplished by slowly rotating the nozzles rearward to accelerate the aircraft and thereby gain aerodynamic lift. When the nozzles reach the cruise position, the aircraft is in conventional flight with nearly all the lift transferred to the wings.

It is well known that a flat surface (such as a wing) with a vertically directed jet of fluid emitting from its center suffers a jet-induced download in proximity to the ground caused by reduced pressures acting on the lower surface (refs. 3 to 4). Recent investigations of some jet VTOL configurations (refs. 5 and 6) have indicated that large induced effects can be experienced in transition from hovering to conventional flight out of the region of ground effect. This mutual interference between the jet exhaust, fuselage-wing combination, and the free-stream flow can result in large lift losses and accompanying nose-up pitching moments at low forward speeds. The jet interference induces pressure increments on the lower surface of the wing (elevated pressures upstream and reduced pressures downstream of the jet with respect to free-stream static pressure). The jet effects diminish with distance, but may extend 10 to 15 jet diameters behind and 5 to 10 diameters to either side of the jet. The reduction of pressures behind the jet is larger and involves more surface area than the increase in pressures ahead of the jet. This effect results in a jet-induced download and accompanying nose-up pitching moment.

The present investigation was undertaken to evaluate further the jet interference problem out of the region of ground effect with a four-jet configuration, and to provide some preliminary data on the effects of wing planform. Nondimensional lift and pitching-moment data are presented as a function of the velocity ratio (free-stream velocity to average jet-exit velocity). Data were obtained for average jet-exit velocities of approximately 670 feet per second and 925 feet per second through a range of free-stream velocities from 0 to 300 feet per second.

SYMBOLS

A_j total nozzle cross-sectional area, sq in.

D_e effective nozzle diameter (diameter of a circle equal in area to total nozzle area), in.

K ratio of measured thrust to calculated thrust, $\frac{T}{T_c} = \frac{V_j}{(V_j)_c}$

L lift, $T + \Delta L$, lb

ΔL increment in lift due to interference, lb

m_j mass rate of airflow through nozzle system, slugs/sec

ΔM	increment of pitching moment due to interference, in-lb
p_t	total pressure in nozzles, lb/sq ft
p_∞	free-stream static pressure, lb/sq ft
R	Reynolds number, based on effective nozzle diameter
S	wing area, sq in.
T_c	calculated thrust, $m_j(V_j)_c$, lb
T	measured thrust, $m_j V_j = KT_c$, lb
V_j	average jet-exit velocity (based on measured thrust and mass flow), $K(V_j)_c$, ft/sec
$(V_j)_c$	calculated average jet-exit velocity (based on isentropic expansion to free-stream static pressure), ft/sec
V_∞	free-stream velocity, ft/sec
α	angle of attack, deg
ζ	skew angle of wing, based on angle of 50-percent-chord line, deg
Λ	outer-panel leading-edge sweep angle, deg

MODEL AND APPARATUS

Details of the model and the various wing planforms tested are shown in figures 1 and 2. The fuselage consisted of a pressure can with four convergent nozzles which were directed vertically downward (normal to the free stream) and were fixed. The nozzle assembly was attached to the mechanical scales at the tunnel ceiling with a streamlined strut through which compressed air was directed to the model (fig. 3).

A simplified fuselage was built around the nozzle assembly and connected to it by three strain-gage beams, one forward and two rearward, to measure the interference force and associated moment. The center section of the fuselage was a split steel shell with clearance provided around the four nozzles and the pressure-can mounting strut. A

sponge-rubber collar was used around the support strut to prevent air from flowing inside the fuselage center section and out the clearance gaps around the nozzles. Because of the small clearance between the fuselage and nozzle system, an electrical circuit was used to detect fouling.

The fuselage center section was built with a flat top on which the various wings were attached. The wings were cut from 1/16-inch steel plate with rounded leading and trailing edges, and were attached to the fuselage at zero incidence angle. The nose and aft fuselage sections were made of mahogany and were simple bodies of revolution.

The mass flow of air through the model was measured by using a calibrated sharp-edge orifice plate located in the incoming air line. Temperature and pressure measurements needed for determining the theoretical jet-exit velocities were made in the pressure can and center of each nozzle, respectively.

TESTS

The tests were conducted at zero angle of attack, zero wing incidence angle, and with the nozzles directed vertically downward. The model was tested in the 7- by 10-foot test section with the center line of the fuselage approximately 24 effective nozzle diameters from the floor (fig. 3).

The data were obtained for average jet-exit velocities of approximately 670 feet per second and 925 feet per second through a free-stream-velocity range from 0 to 300 feet per second in order to obtain overlapping data covering the velocity-ratio range from 0 to about 0.33. The Reynolds number range, based on the effective nozzle diameter, is presented in figure 4 as a function of the velocity ratio and the average jet total-pressure ratio.

CORRECTIONS

A model-misalinement and strut-interference correction was applied to the data by testing the model through a free-stream-velocity range with the jets off and subtracting the recorded lift and pitching moment from the jets-on data.

Tufts were placed on the tunnel floor to determine the conditions under which the jets impinged on the floor. The tufts indicated that

impingement did not occur above a velocity ratio V_∞/V_j of 0.14. Even at the lowest velocity ratio investigated (other than zero), the jet impingement did not cause any flow upstream along the floor. The tunnel-wall effects from this source are believed to be small and are therefore neglected in the results of this investigation. Owing to the small size of the model with respect to the test section, no blockage corrections were applied to the data.

THRUST CALIBRATION

The streamline strut supplying air to the model was exposed to the tunnel airstream during the tunnel-on tests, and therefore it was necessary to establish the nozzle thrust on the basis of the measured mass flow and the nozzle total pressure during the tests. This was accomplished by measuring the mass flow of air in the system with the calibrated sharp-edge orifice plate located in the incoming air line, the temperature in the pressure can, and the total jet pressure in the center of each nozzle. The average of the four total pressures was then used to calculate the jet-exit velocity $(V_j)_c$, based on isentropic expansion to free-stream static pressure; the total thrust T_c, based on this jet-exit velocity, was then calculated. This value of thrust is referred to as the calculated thrust.

Because of the small size of the pressure chamber that could be mounted inside the model, the flow from each nozzle was not uniform but somewhat peaked at the center. This resulted in high values of the average nozzle total pressure and consequently in high values of the calculated jet velocity and thrust. It was necessary, therefore, to establish a thrust calibration factor for the nozzle system for use in the tunnel-on tests. The measured thrust T was obtained with the tunnel air off by measuring the total force on the mechanical scales and individual strain-gage beams and adding the jet-induced download to the scale reading. This value of thrust is plotted as a function of the calculated thrust T_c and the reference pressure ratio p_t/p_∞ in figure 5. The slope of this variation is the calibration factor K, which is a measure of the efficiency of the nozzle system and the inaccuracy involved in determining T_c, which resulted from the use of only one total-pressure measurement in the center of each nozzle in computing the jet velocity. The mass rate of airflow through the model was measured independently of the average nozzle total pressure, and therefore the calibration factor is also equal to the ratio of the average jet-exit velocity based on the measured thrust to the average jet-exit velocity based on isentropic expansion to free-stream static pressure. The measured thrust T and the average

jet-exit velocity based on this thrust, $V_j = K(V_j)_c$, was used in the analysis of the data.

The total-pressure tubes indicated the thrust division in the nozzle system and showed a velocity variation between nozzles. The only effect on the data from this variation of jet-exit velocity would be a slight change in the induced load distribution and is believed to be negligible for the purposes of this investigation.

PRESENTATION OF RESULTS

The results of the investigation are presented in the following figures:

RESULTS AND DISCUSSION

Basic Data

The basic data for each configuration are presented in figure 6. The lift, which includes the jet-induced increment, was nondimensionalized by dividing by the primary measured thrust. The increment of pitching moment due to interference is presented nondimensionalized by dividing by the product of the primary measured thrust and the effective nozzle diameter. All the data are presented as a function of the velocity ratio V_∞/V_j, which eliminates the effects of jet total-pressure ratio within the accuracy and scope of the investigation.

Interference Lift

Figures 7 and 8 are comparison plots for the two groups of variable-geometry configurations, the conventional variable-sweep wing at three different outer-panel leading-edge sweep angles and the skewed wings, respectively. A jet-induced download was encountered by all configurations throughout the velocity-ratio range, and is seen to be primarily a function of the amount of wing area surrounding the nozzle system. Folding the wing back over the fuselage reduces the loss in lift because it reduces the area for the induced pressures to act upon.

The static calibration for the basic nozzle system was performed with the fuselage alone, and an evaluation of the loss due to reduced pressures acting on the bottom surface of the fuselage was obtained. This loss amounted to about 2 percent of the total thrust throughout the pressure-ratio range. By subtracting this increment from the interference lift for each configuration investigated, at $V_\infty/V_j = 0$, the increment of interference lift due to the presence of each wing at zero forward speed could be obtained.

Interference Pitching Moment

The interference pitching-moment parameter as a function of velocity ratio is presented in figures 7 and 8 for the two groups of variable-geometry configurations. The 25° and 75° swept wings (fig. 7) indicate small differences in the interference lift but a large change in nose-up pitching moment at velocity ratios greater than 0.1. At a constant value of V_∞/V_j, sweeping the outer panels to intermediate positions causes a rearward shift in center of pressure. When the wing is folded back over the fuselage, the exposed wing area is greatly reduced and located much closer to the moment reference center; therefore, smaller lift losses and nose-up pitching moments resulted.

The skewed wings (fig. 8) indicate large differences in the interference lift but only small changes in nose-up pitching moment. This result indicates that the interference lift due to the front jets is probably nearly equally divided between areas forward and rearward of the moment reference center.

For a VTOL aircraft with a jet-exit velocity of approximately 1,000 feet per second, transition would be completed at a velocity ratio between 0.1 and 0.2; therefore, the primary area of interest lies at the low velocity ratios. Although the pitching moments appear small, in the region of interest, they nevertheless would require unfavorable control forces and would be a problem in the transition.

Configuration Effects

The results of an investigation of a two-jet arrangement with a large cropped delta wing (refs. 5 and 6) are compared in figure 9 with the variable-sweep configuration at two sweep positions (leading-edge sweep angle of 25° and 75°). The four-jet variable-sweep configurations had a jet-area—wing-area ratio of approximately 2.5 times that of the two-jet arrangement, and indicate a much smaller lift loss and nose-up pitching moment. Inasmuch as the static lift loss for the two-jet configuration could not be determined because of the testing technique employed, this increment is not included in the data for this configuration.

The configuration sketches of figure 9 can be used to discuss the reasons for the large differences in the induced lift and pitching-moment increments. The lift loss is seen to be primarily a function of the amount of wing area surrounding the nozzle system. Since the two-jet configuration has more wing area for the induced pressures behind the nozzles to act upon, it has a much greater lift loss.

The induced pitching-moment increment is seen to be a function of the exposed wing area (area outboard of the fuselage) and also the position of the wing with respect to the nozzle system. The wing of the two-jet configuration is located farther rearward with respect to the nozzle system than is the wing of the four-jet configurations. This location places most of the wing area aft of the nozzles and behind the moment reference center in the region of maximum induced pressures. Thus, a much greater nose-up pitching-moment increment occurs, as is the case with the variable-sweep configurations when the outer panels are rotated aft to intermediate positions. Reference 5 indicates that increasing the wing angle of attack provides enough wing lift to compensate for the jet-induced lift loss throughout the transition; however, the pitching-moment problem remains.

CONCLUDING REMARKS

A limited investigation of the jet interference effects out of the region of ground effect for a four-jet VTOL configuration with various wing planforms has been made. A jet-induced download is encountered by all configurations throughout the velocity-ratio range and is accompanied by a nose-up pitching moment at velocity ratios greater than 0.1. The jet interference effects are seen to be a function of the amount of wing area outboard of the fuselage and its longitudinal position with respect to the nozzle system. Moving the wing aft in relation to the

nozzle system places more wing area behind the moment reference center in the region of maximum induced pressures and thereby results in larger nose-up pitching moments.

Langley Research Center,
National Aeronautics and Space Administration,
Langley Station, Hampton, Va., June 27, 1962.

REFERENCES

1. Luoma, Arvo A.: Longitudinal Aerodynamic Characteristics at Transonic Speeds of Two V/STOL Airplane Configurations With Skewed and Variable-Sweep Wings. NASA TM X-527, 1961.

2. Morris, Odell A., and Foster, Gerald V.: Static Longitudinal and Lateral Aerodynamic Characteristics at a Mach Number of 2.20 of a V/STOL Airplane Configuration With a Variable-Sweep Wing and With a Skewed Wing Design. NASA TM X-521, 1961.

3. Spreemann, Kenneth P., and Sherman, Irving R.: Effects of Ground Proximity on the Thrust of a Simple Downward-Directed Jet Beneath a Flat Surface. NACA TN 4407, 1958.

4. Davenport, Edwin E., and Spreemann, Kenneth P.: Thrust Characteristics of Multiple Lifting Jets in Ground Proximity. NASA TN D-513, 1960.

5. Spreemann, Kenneth P.: Induced Interference Effects on Jet and Buried-Fan VTOL Configurations in Transition. NASA TN D-731, 1961.

6. Spreemann, Kenneth P.: Investigation of Interference of a Deflected Jet With Free Stream and Ground on Aerodynamic Characteristics of a Semispan Delta-Wing VTOL Model. NASA TN D-915, 1961.

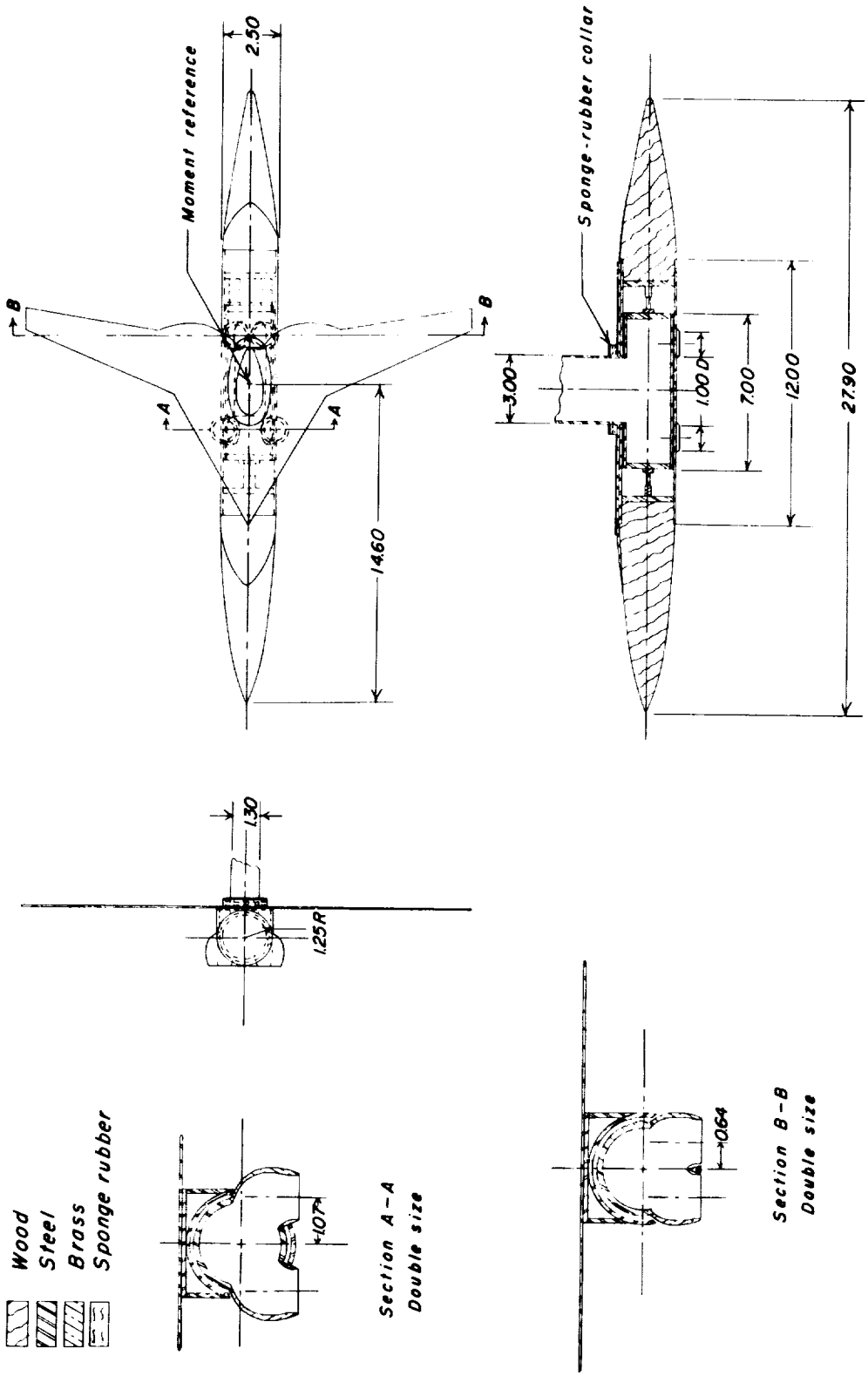

Figure 1.- Model details. All dimensions in inches unless otherwise noted.

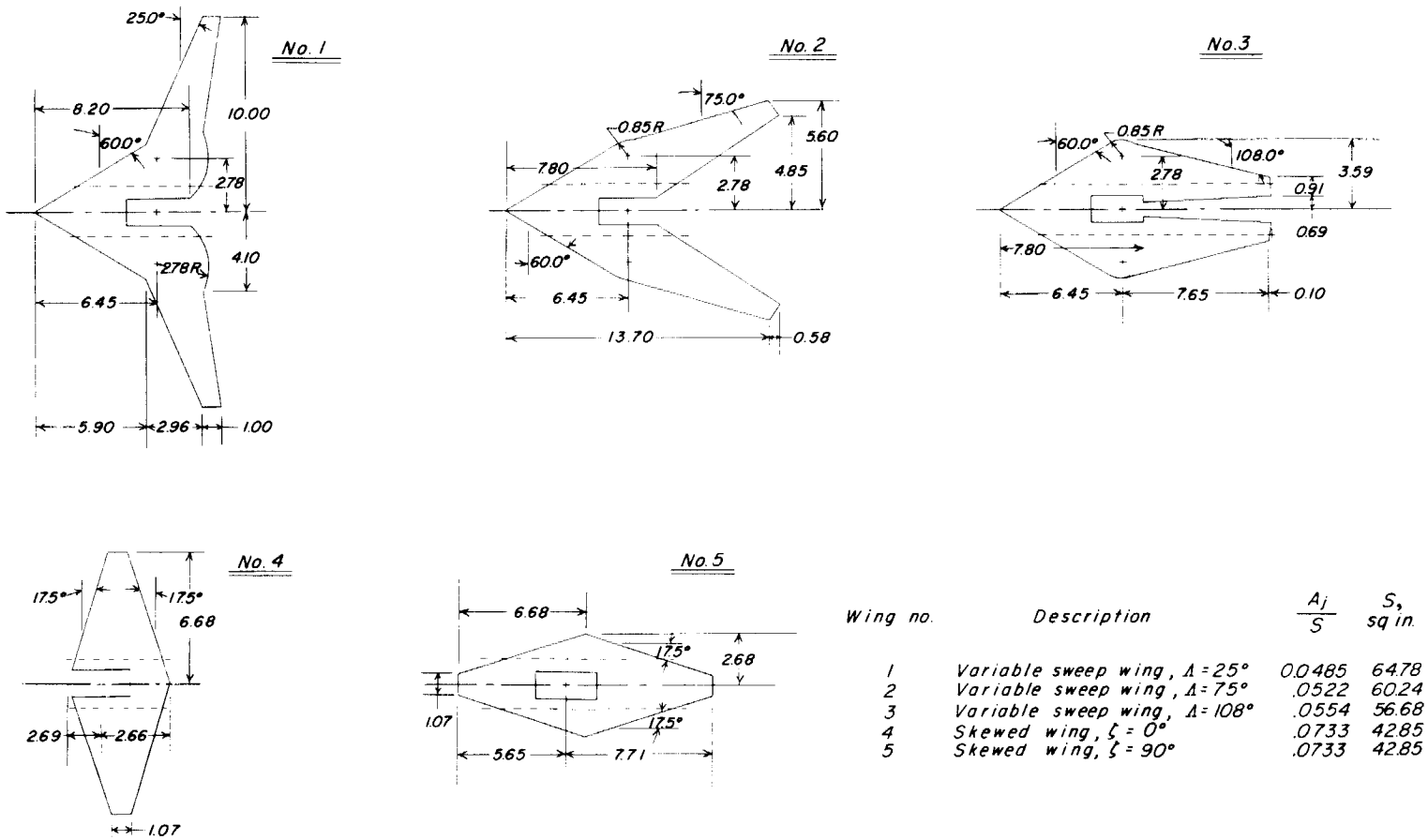

Wing no.	Description	$\frac{A_j}{S}$	S, sq in.
1	Variable sweep wing, $\Lambda = 25°$	0.0485	64.78
2	Variable sweep wing, $\Lambda = 75°$	.0522	60.24
3	Variable sweep wing, $\Lambda = 108°$	.0554	56.68
4	Skewed wing, $\zeta = 0°$	.0733	42.85
5	Skewed wing, $\zeta = 90°$	.0733	42.85

Figure 2.- Drawing of the wing planforms tested. All dimensions in inches unless otherwise noted.

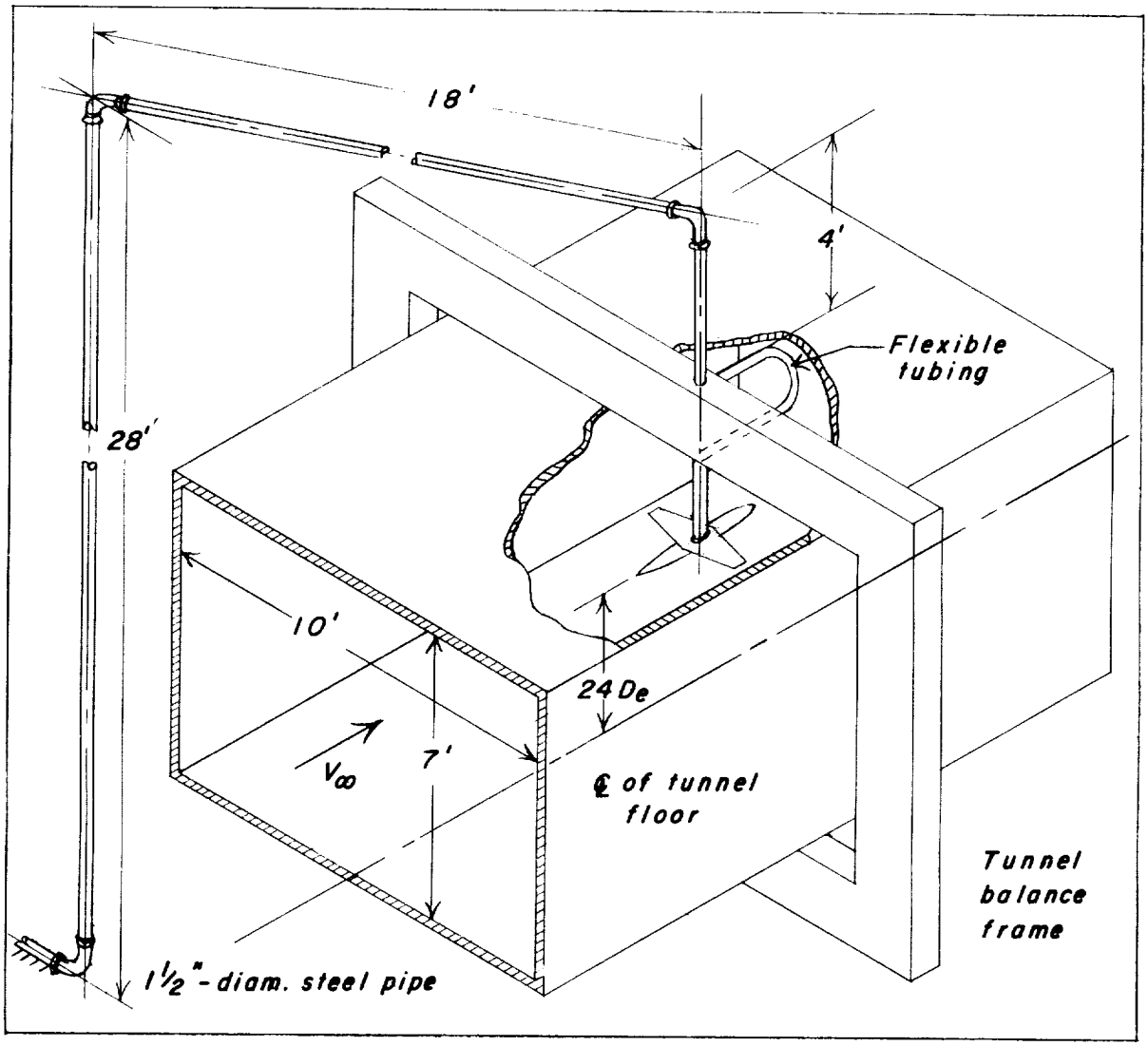

Figure 3.- Schematic diagram of method used to introduce high-pressure air to the model.

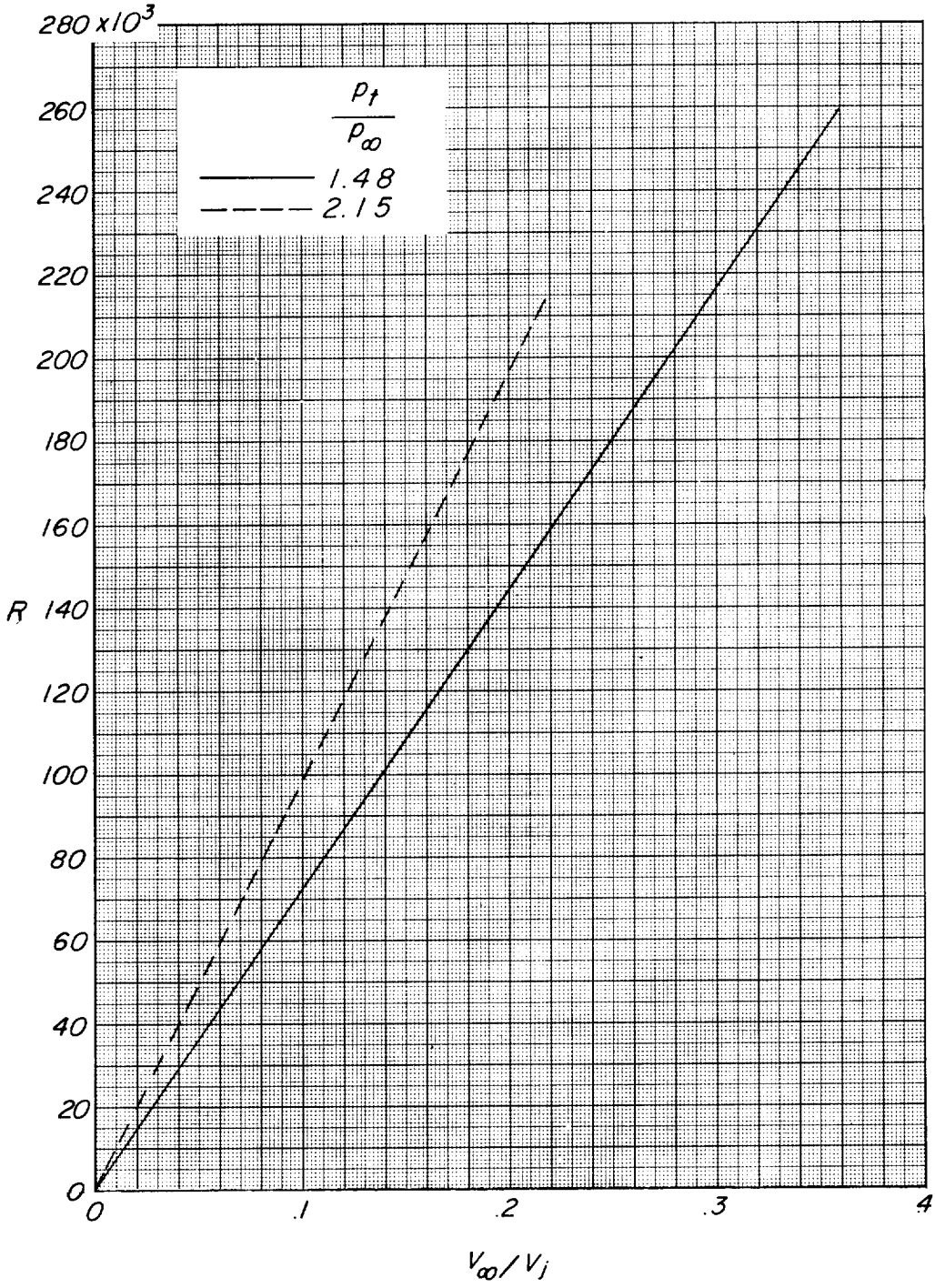

Figure 4.- Variation of Reynolds number with velocity ratio for two jet total-pressure ratios.

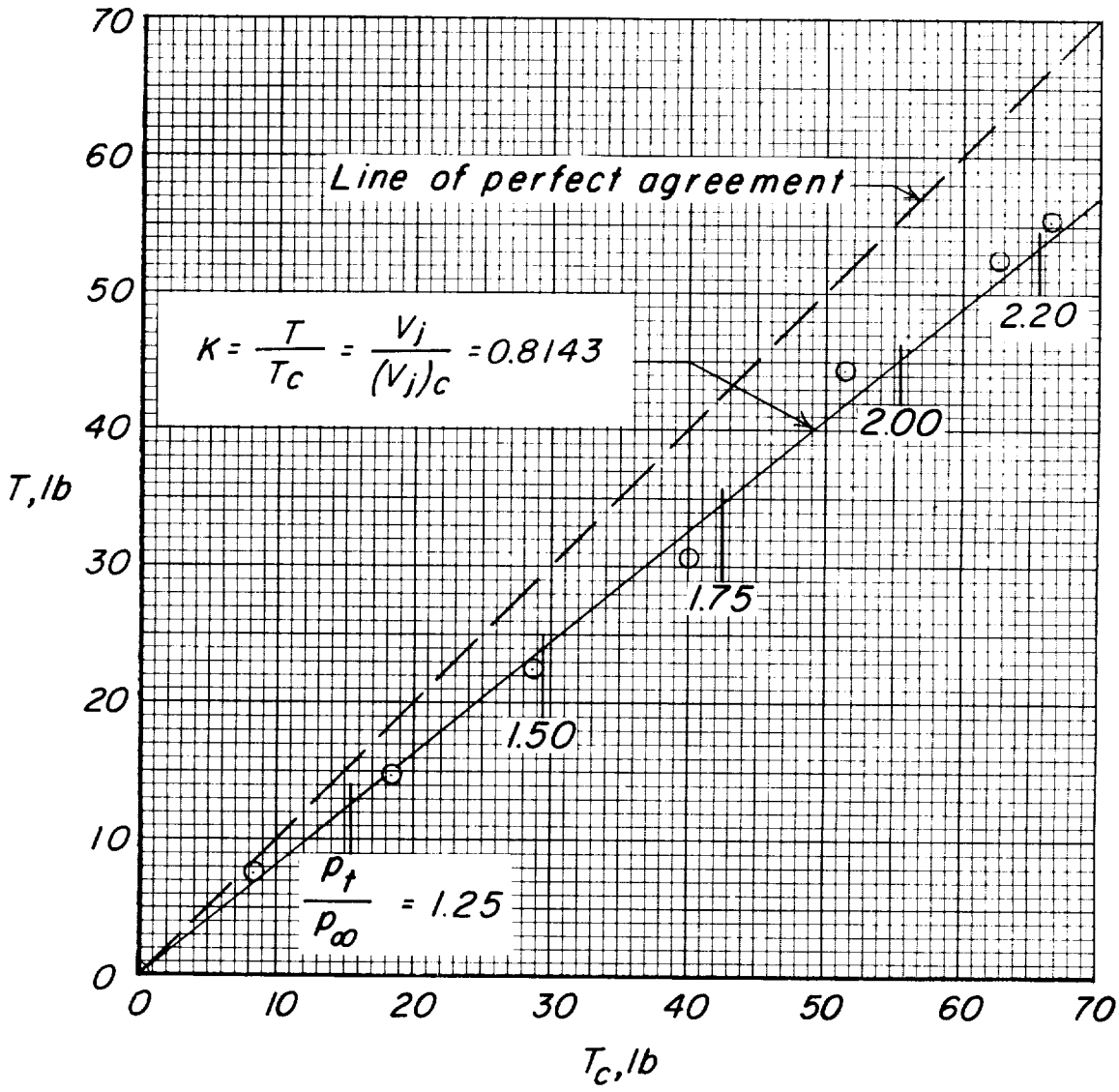

Figure 5.- Variation of measured thrust with calculated thrust for the complete nozzle system. $V_\infty = 0$.

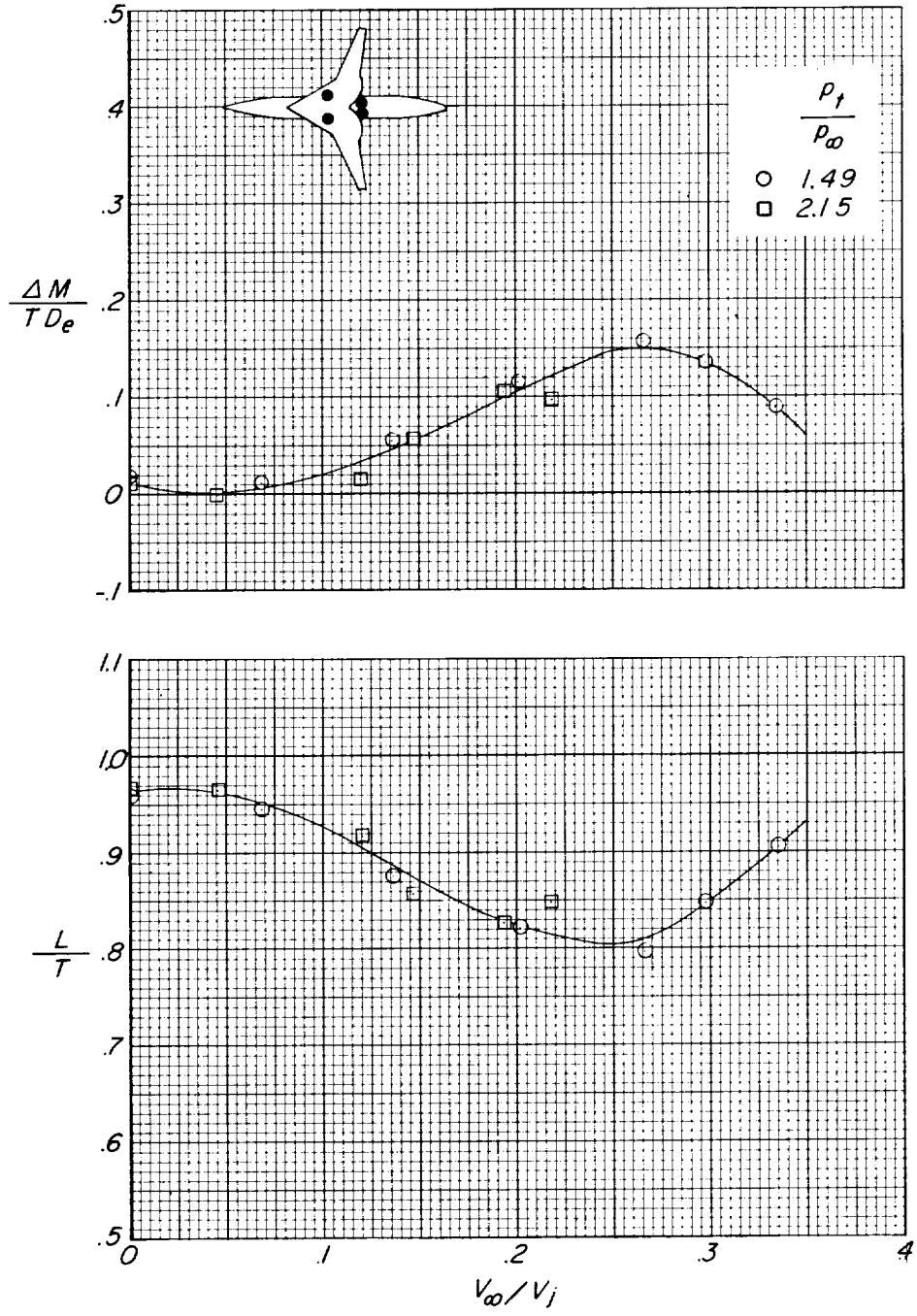

(a) Variable-sweep wing. $\Lambda = 25^{\circ}$.

Figure 6.- Nondimensional lift and pitching-moment parameters as a function of the velocity ratio. $\alpha = 0^{\circ}$.

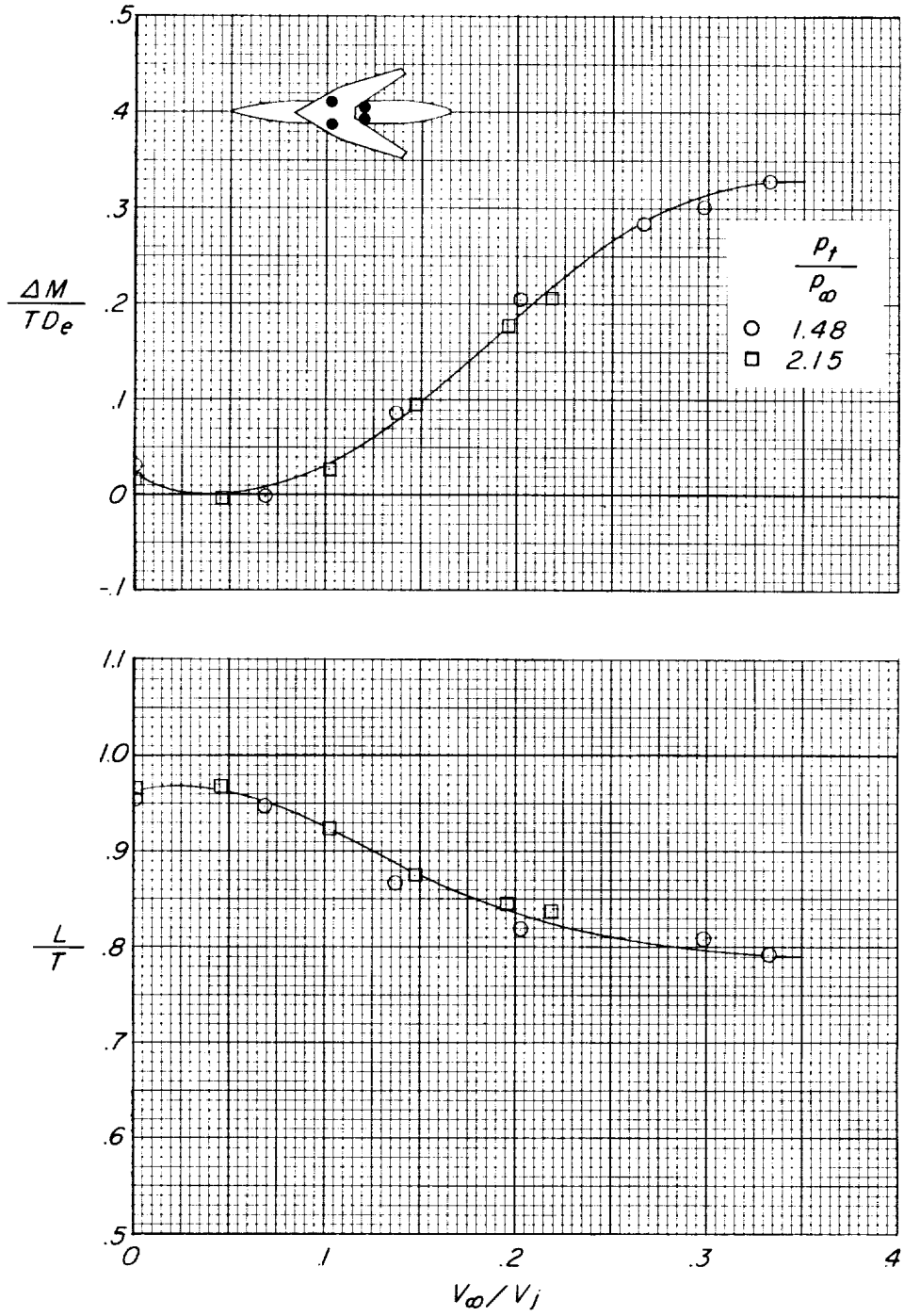

(b) Variable-sweep wing. $\Lambda = 75^{\circ}$.

Figure 6.- Continued.

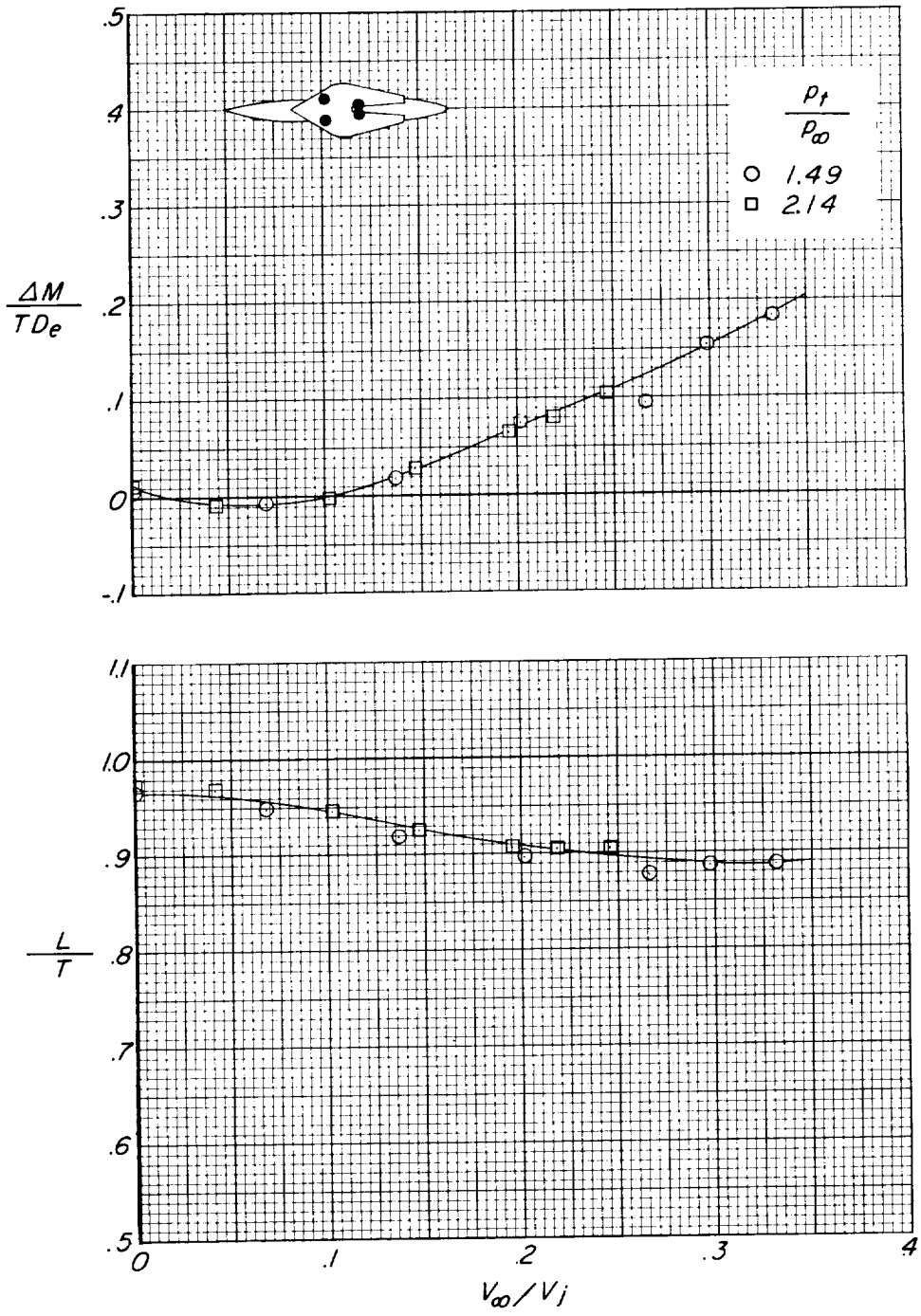

(c) Variable-sweep wing. $\Lambda = 108^\circ$.

Figure 6.- Continued.

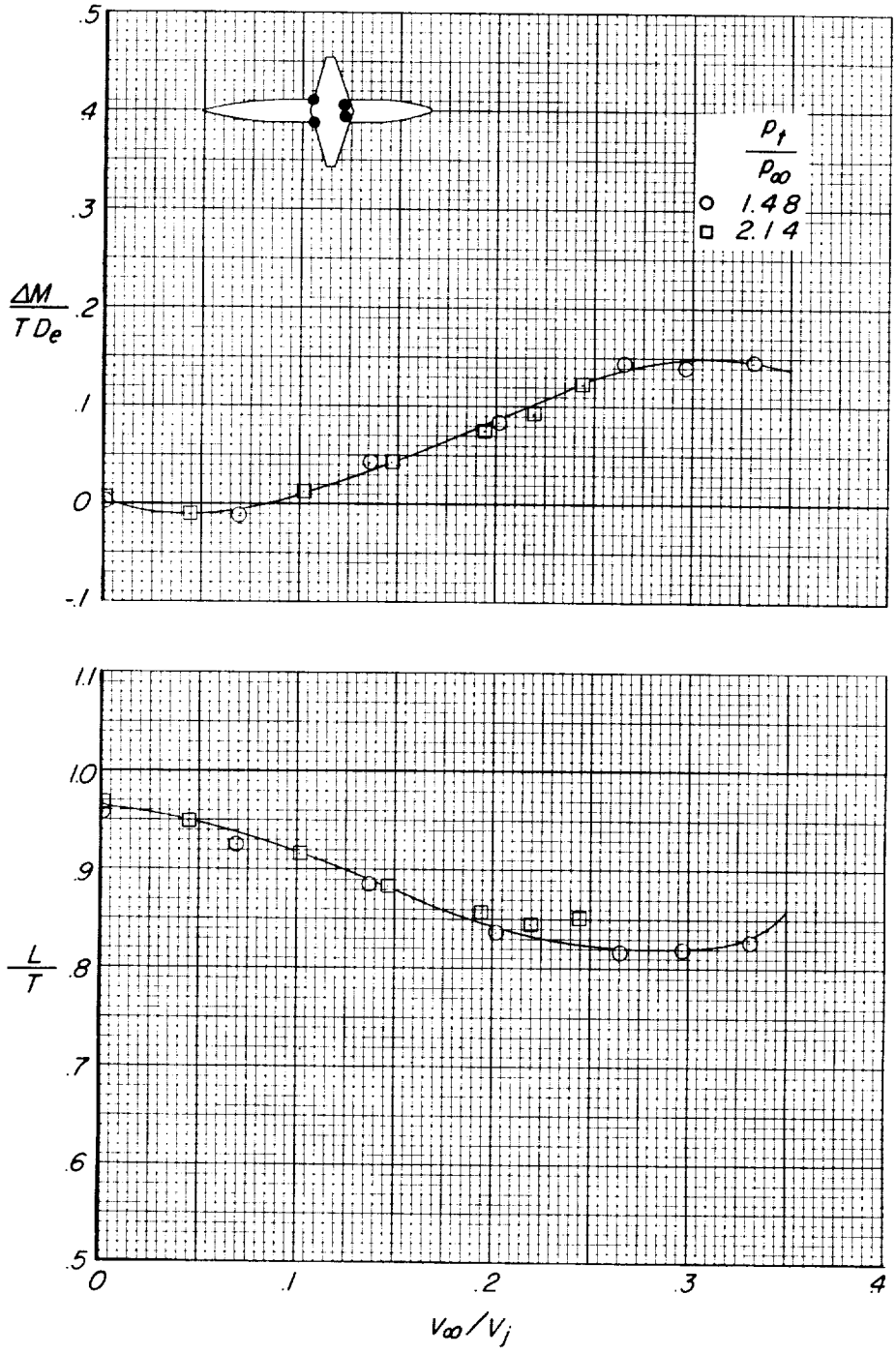

(d) Skewed wing. $\zeta = 0^{\circ}$.

Figure 6.- Continued.

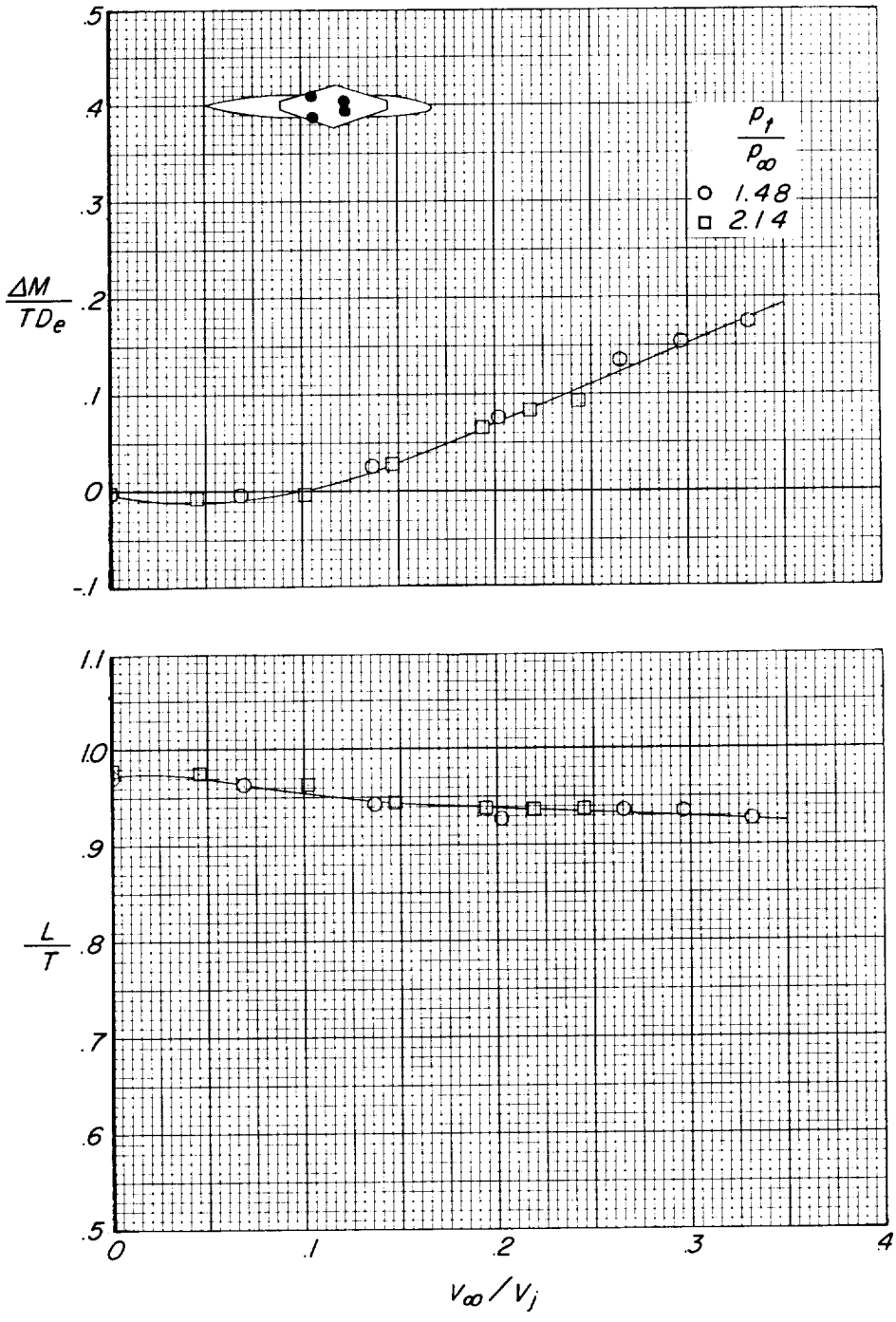

(e) Skewed wing. $\zeta = 90^{\circ}$.

Figure 6.- Concluded.

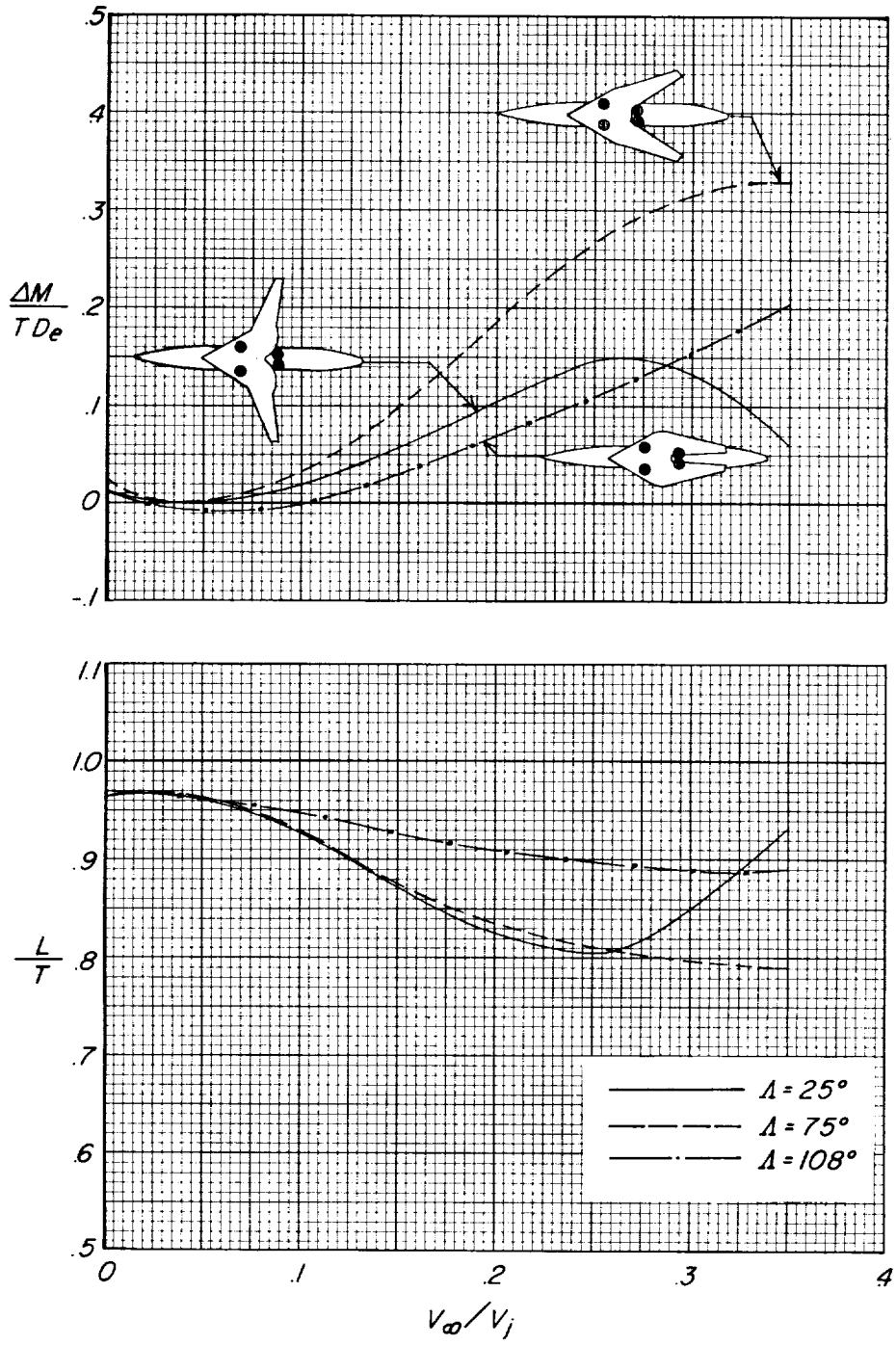

Figure 7.- Comparison of the nondimensional lift and pitching-moment parameters as a function of the velocity ratio for the variable-sweep wings. $\alpha = 0^{\circ}$.

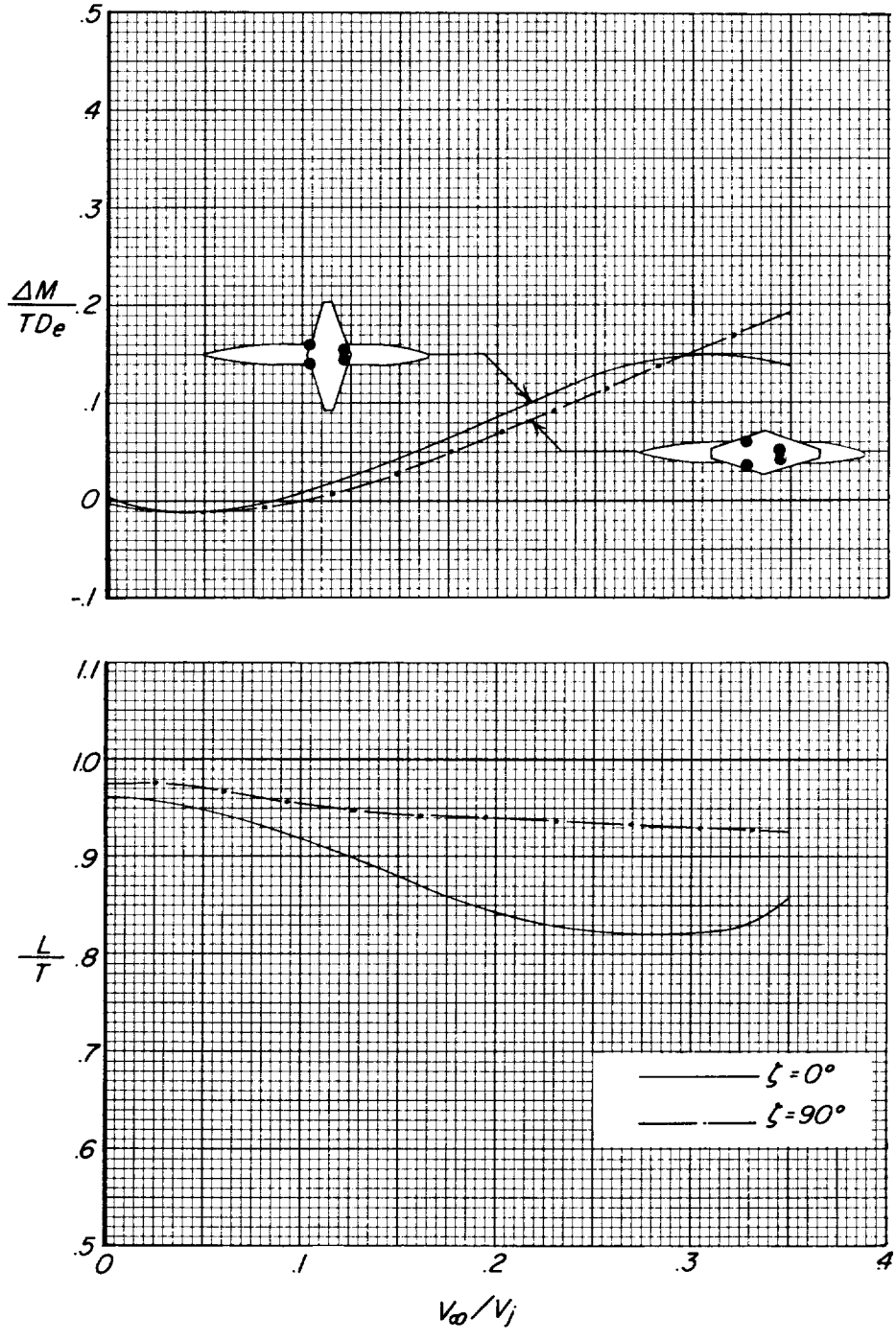

Figure 8.- Comparison of the nondimensional lift and pitching-moment parameters as a function of the velocity ratio for the skewed wings. $\alpha = 0^{\circ}$.

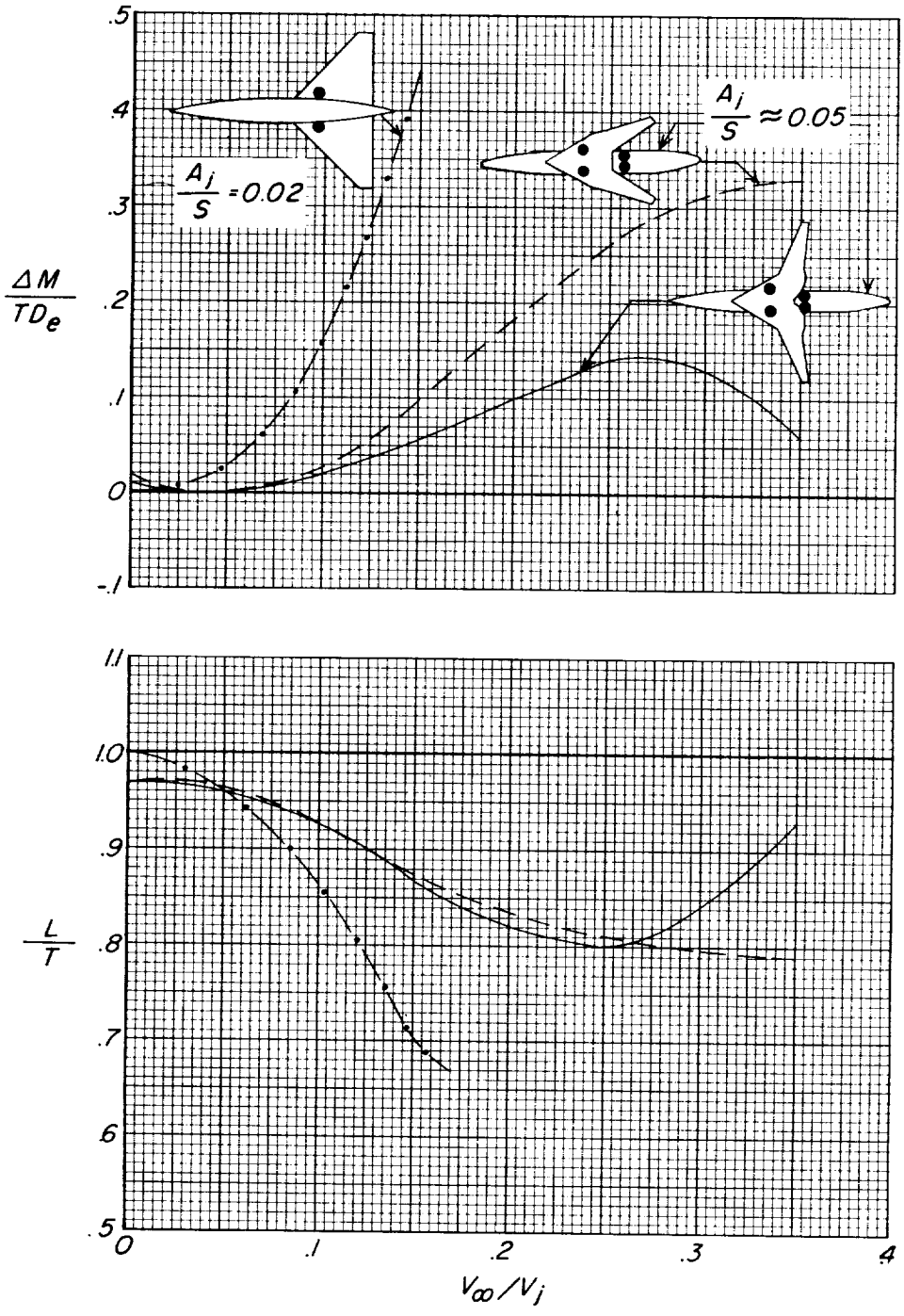

Figure 9.- Comparison of the nondimensional lift and pitching-moment parameters for a two-jet configuration (refs. 5 and 6) and two different four-jet configurations. $\alpha = 0^\circ$.